Korean Journal of Remote Sensing, Vol.17, No.4, 2001, pp.335~344

Contextual Modeling and Generation of Texture Observed in Single and Multi-channel Images

Myung-Hee Jung

Dept. of Digital Media, Anyang University, Korea

Abstract : Texture is extensively studied in a variety of image processing applications such as image segmentation and classification because it is an important property to perceive regions and surfaces. This paper focused on the analysis and synthesis of textured single and multiband images using Markov Random Field model considering the existent spatial correlation. Especially, for multiband images, the cross-channel correlation existing between bands as well as the spatial correlation within band should be considered in the model. Although a local interaction is assumed between the specified neighboring pixels in MRF models, during the maximization process, short-term correlations among neighboring pixels develop into long-term correlations. This result in exhibiting phase transition. In this research, the role of temperature to obtain the most probable state during the sampling procedure in discrete Markov Random Fields and the stopping rule were also studied.

Key Words : Texture, Markov Random Field, PhaseTransition, Annealing Algorithm, Contextual Model.

1. Introduction

Texture can be considered to be as stochastic, possibly periodic, two-dimensional image field and gives inherent features and information on orientation of an object. With this reason, texture analysis and synthesis have been extensively studied and utilized for a variety of image processing applications such as image segmentation and classification in remote sensing, biomedical image analysis, and automatic detection of surface defects. In many researches, statistical approaches has been utilized and resulted in development of many practical algorithms for texture analysis. Among them, random fields have been successfully used to sample and synthesize textures during several decades.

Random field is a joint distribution of pixel intensities that imposes statistical dependence in a spatially meaningful way. Markov random field (MRF) is a very natural stochastic model of texture that can extend local information and assumption into a global model. It has been consequently utilized in many applications such as problems in texture modeling and classification (Cross and Jain, 1983; Solberg, 1999) and research in

Received 29 Octobet 2001 ; Accepted 25 November 2001.

segmentation (Derin and Elliot, 1987, and Dubes and Jain, 1989), permitting the introduction of spatial context.

This paper focused on modeling and generating single and multiband textured image using both discrete and continuous MRF. MRF models *priori* beliefs about the textural spatial continuity and maximizes the resulting posterior distribution in a Bayesian framework making analysis mathematically tractable. Texture analysis of the multiband imagery acquired over ranges of frequency are utilized in many applications such as classification, segmentation and restoration of remote sensing data and color imagery. For modeling and generating textured multichannel images, Gaussian Markov Random Field (GMRF) is utilized, which is a special case of MRF where pixel values have jointly Gaussian distributions.

A variety of relaxation-type algorithms have been developed based on a Monte Carlo computational theory to obtain the most probable state such as an annealing algorithm. In MRF models, each pixel is assumed to have a local interaction with the specified neighbors that is independent of the location in the image. However, during the maximization process, short-term correlations among neighboring pixels develop into long-term correlations, exhibiting phase transition [Geman and Geman, 1984]; that is, as parameter values increase past critical values, abrupt changes in qualitative behavior occur. Thus, site variables lose their asymptotic independence, which leads distortion and limits statistical inference.

The temperature is utilized as an annealing parameter to obtain the most probable state avoiding the phase transition. The process is terminated when the pattern has stopped changing after some number of iterations. The proper stopping rule needs to be defined for the number of iterations required to stop the algorithm. In this study, the effect of temperature was also investigated.

This paper is organized as follows: Section II describes the contextual models for texture. The phase transition in MRF and the stopping rule of the annealing process for the most probable state is explored in Section III. Section IV includes the evaluation of the proposed method and some results. Finally, Section V has some conclusions

2. Contextual Modeling for Texture

1) Utilization of Discrete Markov Random Field

A random field model is a specification of a probability measure for a particular class of random variables such as those representing intensities or depth values of pixels in an image. All images are defined on an $N_1 \times N_2$ rectangular lattice,

$$L = \{(i, j); 1 \le i \le N_1,\ 1 \le j \le N_2\}.$$

A proposed random field $\mathbf{X}=\{X_i\}$ defined on L has a Gibbs Distribution (GRF) with the joint distribution of the following form,

$$P(x=\omega) = \frac{1}{Z} e^{-U(\omega)/T}, \qquad (1)$$

where $U(\omega)= \sum_{all\ c} V_c(\omega)$,which is called energy function, and $Z=\sum e^{-U(\omega)}$ is simply a normalizing constant. The clique function, $V_c(\omega)$, associated with each clique depends only on the values at sites in clique c and represents contributions to the total energy: for single clique function, $V_c(\omega) = \alpha_k$ if pixel value in clique c is equal to k, and for pairwise clique function, $V_c(\omega) = h \cdot \beta_{dir}$ where $h =$

-1 if all pixel values in clique c are equal, $h=1$ if not, and *dir* means four types of direction between pixels (NE, SW, NE(SW), NW(SE)). Paramters, α and β's, control the percentage of each pixel value and clustering of pixels in each direction, respectively. T, temperature, is utilized as an annealing parameter.

Since the partition function Z is practically intractable, standard statistical procedures can't be employed and relaxation-type algorithms are utilized to eliminate the need for computing the partition function.

2) Utilization of Continuous Markov Random Field

Since multispectral data contain interchannel correlation, both the cross-channel correlation existing between frequency bands and statistical dependence between neighboring pixels should be considered in the model.

In the GMRF model for multichannel images, the intensity at each pixel is represented as a linear combination of all the neighboring intensities in the multiple channel and additive correlated noise. A Gaussian Markov model defined for p multiple channels can be described:

$$\mathbf{z}(s) = \sum_{r \in N_s} \Theta_r \mathbf{z}(s+r) + \mathbf{e}(s) \qquad (2)$$

where $\mathbf{z}(s)$ and $\mathbf{z}(s+r)$ representing a pixel vector at location s and its spatially meaningful neighboring vector, respectively,

$$\mathbf{z}(s) = (z_1(s), z_2(s), \cdots, z_p(s))^T$$

$$\mathbf{z}(s+r) = (z_1(s+r), z_2(s+r), \cdots, z_p(s+r))^T$$

and Θ_r is the parameter set representing the statistical dependence of a pixel value on those values in its neighboring pixels within band and between bands. The noise vector $\mathbf{e}(s)$ is Gaussian with zero mean and covariance matrix Σ and its correlation structure is defined as follows:

$$E(\mathbf{e}(s)\mathbf{e}(r)) = \begin{cases} \Sigma & s=r \\ -\Theta_{s-r}\Sigma & (s-r) \in N_s \\ 0 & otherwise \end{cases} \qquad (3)$$

where N_s is the symmetric neighbor set considering both the spatial interaction within a band and the interaction between bands.

Since the maximum likelihood estimates to maximize the log-likelihood function, $P(\mathbf{z} \mid \Theta, \Sigma)$ is computationally difficult, herein, least square estimates obtained by maximizing the pseudolikelihood are utilized as computationally efficient estimation scheme in the following (Chellapa, 1985).

$$L = \prod_{s \in S_I} \frac{1}{(8\pi^3|\Sigma|)^{1/2}} \exp\left\{-\frac{1}{2}(\mathbf{z}(s) - \sum_{r \in N_s} \Theta_r \mathbf{z}(s+r))^T \Sigma^{-1} (\mathbf{z}(s) - \sum_{r \in N_s} \Theta_r \mathbf{z}(s+r))\right\} \qquad (4)$$

where S_I is the interior set of S such that $S_I = S - S_B$ where S_B is the boundary set in the outer block of the image.

3) Sampling of MRF

Textures with the specified parameters are generated using sampling method. Sampling is the process of generating a realization of a random field, given a model whose parameters have been specified or estimated. For it, relaxation-type algorithm are utilized which simulates a Markov chain through an iterative procedure that readjusts the gray levels at pixel location during each iteration (Geman and Geman, 1984): a single pixel location is selected at random and using the conditional distribution that describes the Markov chain, $P(\mathbf{z}(s) \mid \mathbf{z}(s+r), r \in N_s)$, the new gray level at that location is selected dependent only upon the gray levels of

the pixels in its local neighborhood. The sequential algorithm terminates after a given number of iterations.

There have been various constructions of Markov chains that possess a Gibbs invariant distribution and whose common characteristic is that their transition probabilities depend only on the ratio of the Gibbs probabilities. In GMRF, the continuous Gaussian distribution is utilized as the probability function. Actually, it takes a lot of iteration before stable texture is obtained. GMRF can also be generated by the efficient scheme that uses 2D Fourier transforms and doesn't need iteration (Picard *et al.*, 1991).

3. Temperature Effect and Stopping Rule

In sampling using simulated annealing, theoretically, convergence of the process is assured if Niter is large enough when the initial state is chosen randomly. However, the tendency of sampling algorithms to produce uni-color images has been noted in the statistical literature. Unfortunately, experiments have shown that stopping the algorithm too soon may lead to a misleading realization which does not match a MRF with given parameters. Therefore, the number of raster scans, N_{iter} is an important parameter.

Markov random fields exhibit phase transition (Picard, *et al.*, 1991). Short-term correlations among neighboring pixels develop into long-term correlations, which leads distortion. The subset of the parameter space that prevents a discrete Gibbs random field model from experiencing phase transition is unknown. This is one of the difficult problems in defining models. When phase transition occurs, as an alternative, it is suggested that the parameter N_{iter} be selected based on visual interpretation, estimated parameters and proportion of each class for the proper stopping rule.

T is adapted to avoid phase transition and isolate the most probable state (Geman and Geman, 1984) by gradually reducing it according to some cooling algorithm. Typically,

$$T(k)=\frac{c}{\log(1+k)},\ 1 \le k \le K \tag{5}$$

where k is the iteration number and $T(k)$ is the temperature during the kth iteration. The number of iterations performed at each temperature $T(k)$ for the pattern to equilibrate is k_{inner}. Since the pixels were visited in a raster scan, the total number of raster scans during the synthesis is $K \cdot k_{inner}$. The scale factor c controls the annealing progress and is usually selected in (0,10).

The process is terminated when the pattern has stopped changing after some number of iterations. The stopping rule needs to be defined properly for the number of iterations required to stop the algorithm. In this study, both the number of pixels swapping and the similarity between two successive patterns are considered. For this,

$$\begin{aligned} &N^t{}_{swapping}/M < \varepsilon_1 \\ &|N^{t+1}{}_{swapping} - N^t{}_{swapping}|/M < \varepsilon_2 \end{aligned} \tag{6}$$

where $N^t{}_{swapping}$ is the average number of swapping at the temperature t and M is the total number of pixels in the image. The difference between estimated parameters of the samples and the desired parameters is also checked.

4. Experiments

In this section, models for texture are tested

visually and numerically and temperature effect and phase transition in sampling were also explored. For sampling, the Gibbs Sampler is utilized which generates realization by site-replacement algorithms. In the case that a histogram constraint is reasonably assumed, the Metropolis exchange algorithm is a good choice since each class occupies a certain percentage in the image at all times (Dubes and Jain, 1989).

Some examples of texture realizations generated using the Gibbs distribution are presented in Fig. 1, where the response of the model to variation in parametric information such as orientation is demonstrated. All are 128x128 in size with $\alpha_i = 0$ when the values of the β's used in each simulation are specified. The parameters of a specific realization of a Gibbs Random Field (GRM) are estimated using the Least Square Error Method (LSQR) which uses the histogram technique (Derin and Elliot, 1987). Several examples of the parameters estimated are presented in Fig. 2. For this, 1) generate realizations of Gibbs distribution with specific values of parameters ((a) and (c)) in Table 1, 2) estimate parameters from a given realization and compare them to the specified values in Table 1, and then 3) generate realizations with the estimated values of parameter and visually compare them to the original realizations ((b) and (d)). Possible lack of convergence in the realization algorithm may be one cause and the lack of sufficient data can be another factor for deviation in the estimated values because image size 128x128 may be small for LSQR technique.

Here, sampling starts with a randomly chosen initial pattern since the initial state doesn't affect

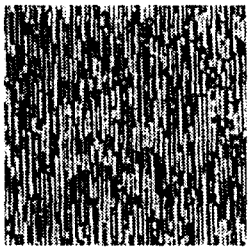

(a) Four gray level with
$\beta_{hor,i} = -1.2, \forall I$
$\beta_{ver,i} = 1.2, \forall I$
$\beta_{ne,i} = -1.2, \forall I$
$\beta_{nw,i} = -1.2, \forall I$

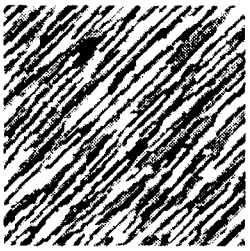

(b) Three gray level with
$\beta_{hor,i} = -1.0, \forall_i$
$\beta_{ver,i} = 1.0, \forall_i$
$\beta_{ne,i} = 1.0, \forall_i$
$\beta_{nw,i} = 1.0, \forall_i$

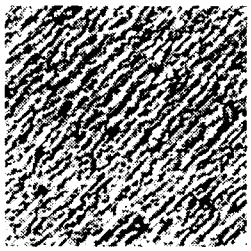

(d) Three gray level with
$\beta_{hor,1} = 0.3, \beta_{hor,2} = 0.5, \beta_{hor,3} = 0.7$
$\beta_{ver,1} = 0.3, \beta_{ver,2} = 0.5, \beta_{ver,3} = 0.7$
$\beta_{ne,1} = 0.3, \beta_{ne,2} = 0.5, \beta_{ne,3} = 0.7$
$\beta_{nw,1} = 0.3, \beta_{nw,2} = 0.5, \beta_{nw,3} = 0.7$

Fig. 1. Some examples of 128x128 texture realizations from discrete MRF model.

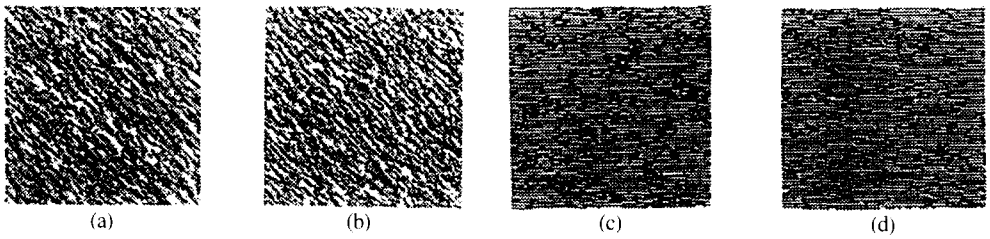

(a) (b) (c) (d)

Fig. 2. Images generated with specified ((a), (c)) and estimated parameters ((b), (d))

Table 1. Specified and estimated parameters for Fig. 2

Figure	Description	Size	class	β_{hor}	β_{ver}	β_{ne}	β_{nw}
(a)	specified	128x128	all classes	0.4	0.4	-0.3	0.6
(b)	estimated	128x128	class 1	0.44	0.34	-0.3	0.58
			class 2	0.43	0.24	-0.28	0.58
			class 3	0.42	0.40	-0.32	0.57
			class 4	0.32	0.32	-0.32	0.57
(c)	specified	128x128	all classes	0.7	-0.7	-0.7	-0.7
(d)	estimated	128x128	class 1	0.77	-0.38	-0.37	-0.46
			class 2	0.67	-0.39	-0.38	-0.42
			class 3	0.81	0.02	-0.81	0.41

the convergence. Convergence of the algorithm is assured if the number of iterations, N_{iter}, is large enough, although it is a critical parameter. Fig. 3 illustrates the effect of N_{iter} in sampling and shows phase transition for various iteration numbers. Terminating the algorithm too soon result in misleading realizations.

Fig. 4 shows the pattern formation according to the different k_{inner} executed at each temperature. Even when it approximates a sample of the Gibbs distribution at a given temperature, image continues to change as T is reduced. At high temperatures, since all gray levels are equally likely at a given pixel, a random-looking pattern is obtained, and as the temperature is lowered, it tends to be a more regulated pattern. Here, it is noted that if a large value for kinner is selected, the image makes many changes quickly, is trapped on the local minimum at the given temperature, and thus doesn't realize the full advantage of annealing.

The process is terminated when the pattern has stopped changing after some number of iterations. For stopping rule, the swapping number per iteration was considered with the similarity between two successive patterns as described in

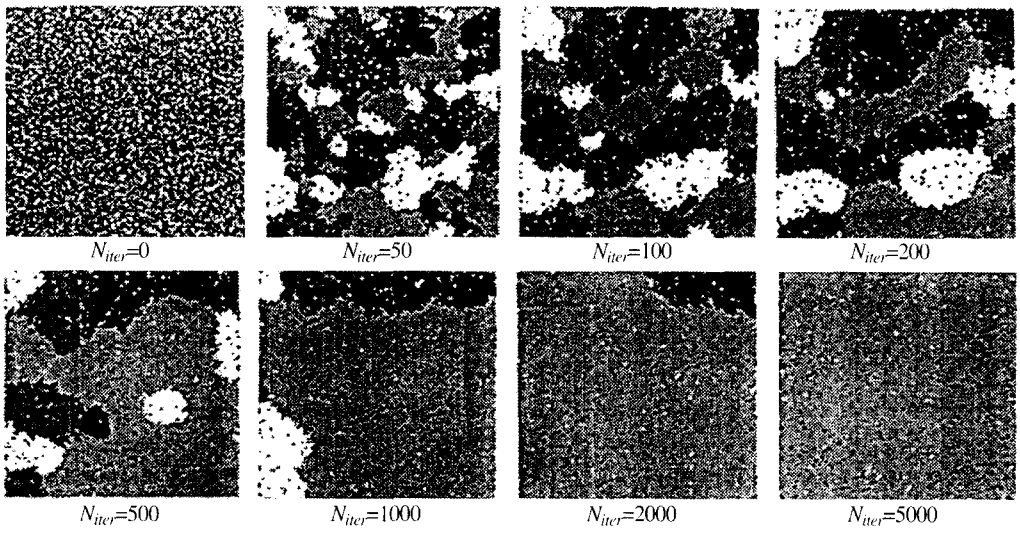

Fig. 3. Phase transition example during sampling process:128x128 4-valued image with $\alpha_k = 0$, $\beta_{ij} = 0.3$, $\forall_{i,j}$.

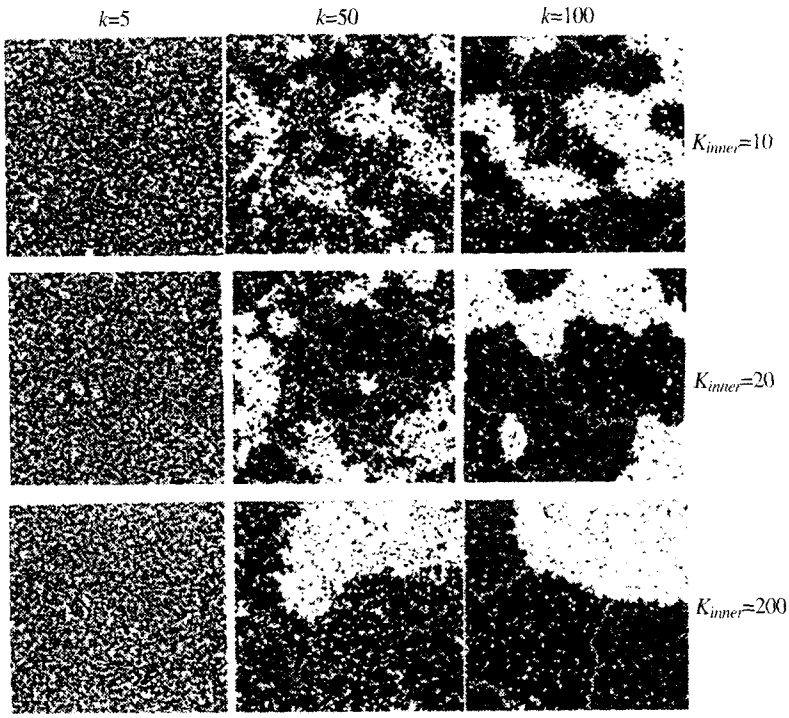

Fig. 4. Effect of the numbers of inner loops, k_{inner} on pattern formation: 128x128 image with $\alpha_i = 0$, $\beta_{ij} = 0.7$, $\forall_{i,j}$

Eq. (6). The Less pixels swap, the similar the successive patterns are. Fig. 5 shows the behavior of percentage of pixels swapped at every iteration obtained by the simulation of images with $\beta_{ij} = 0.7, \forall i, j$ using the Gibbs sampler.

As seen in the experimental results, temperature is to be adapted with a simulated annealing schedule to obtain the pattern that globally minimize the Gibbs energy, since at a given temperature, the patterns that are most likely to be sampled are the ones that locally minimize the Gibbs energy. To avoid phase transition above which all patterns generated will be visually similar and get the most probable state of a realization, the proper iteration number needs to be selected during annealing schedule.

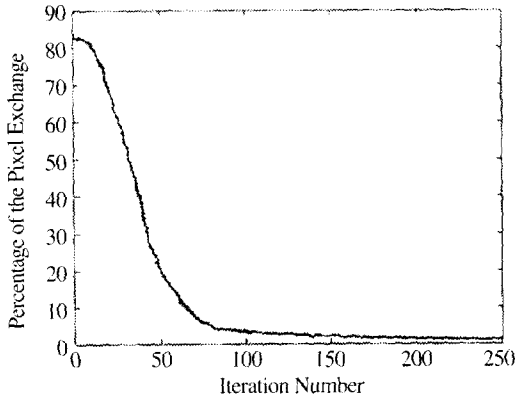

Fig. 5. Evolution of exchange percentage for Gibbs Sampler.

Next, some multiband textured images were generated using GMRF model considering within-channel spatial correlationas well as interchannel correlation. First, in Fig. 6, image (a) and (c) are taken from remotely sensed data (TM data) as examples of continuous random fields. Then, the Least Square Estimates of GMRF model for these real samples were obtained by maximizing the pseudolikelihood as described in section 2 and the estimated values are represented in Table 2. For

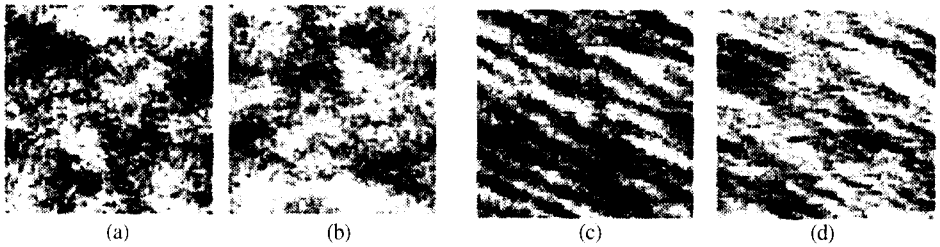

(a) (b) (c) (d)

Fig. 6. Images generated with specified ((a), (c)) and estimated parameters ((b), (d)).

the sake of visual comparison with the original realizations, the corresponding realizations were generated in Fig 6. (b) and (d), respectively. Then, the parameters were reestimated from these generated realizations and compared with the original values in Table 2. Herein, the performance of the algorithm for generating the textured mutiband images can be evaluated visually as well as by comparison of the estimated parameters with the original parameters.

A first order neighborhood model is utilized in image (a), while a second neighborhood model is employed in image (c) where a diagonal effect is shown. It is also recognized that the image (c) has

Table 2. Specified and estimated parameters for Fig. 6.

(a) $\mu = (33.74,\ 48.95,\ 20.63)$

$$\Sigma = \begin{pmatrix} 1.450 & 0.630 & 0.272 \\ 0.630 & 3.406 & 0.741 \\ 0.274 & 0.741 & 0.780 \end{pmatrix}$$

$$\Theta_1 = \begin{pmatrix} 0.240 & 0.026 & -0.007 \\ 0.034 & 0.279 & 0.032 \\ -0.006 & 0.112 & 0.289 \end{pmatrix}$$

$$\Theta_2 = \begin{pmatrix} 0.157 & 0.046 & -0.001 \\ 0.028 & 0.141 & 0.007 \\ -0.017 & -0.002 & 0.156 \end{pmatrix}$$

(b) $\mu = (33.18,\ 48.28,\ 20.14)$

$$\Sigma = \begin{pmatrix} 1.453 & 0.532 & 0.248 \\ 0.532 & 3.073 & 0.676 \\ 0.248 & 0.676 & 0.888 \end{pmatrix}$$

$$\Theta_1 = \begin{pmatrix} 0.212 & 0.019 & -0.007 \\ 0.024 & 0.227 & 0.031 \\ 0.035 & 0.160 & 0.354 \end{pmatrix}$$

$$\Theta_2 = \begin{pmatrix} 0.157 & 0.046 & -0.001 \\ 0.028 & 0.141 & 0.007 \\ -0.017 & -0.002 & 0.156 \end{pmatrix}$$

(c) $\mu = (106.66,\ 45.39,\ 90.19)$

$$\Sigma = \begin{pmatrix} 3.608 & 0.540 & 0.009 \\ 0.540 & 0.900 & 0.023 \\ 0.009 & 0.023 & 2.356 \end{pmatrix}$$

$$\Theta_1 = \begin{pmatrix} 0.428 & 0.037 & -0.030 \\ 0.040 & 0.267 & 0.016 \\ -0.023 & -0.003 & 0.071 \end{pmatrix}$$

$$\Theta_2 = \begin{pmatrix} 0.227 & 0.012 & 0.020 \\ -0.065 & 0.053 & 0.074 \\ 0.050 & 0.039 & 0.094 \end{pmatrix}$$

$$\Theta_3 = \begin{pmatrix} -0.169 & -0.030 & -0.003 \\ -0.006 & 0.020 & 0.032 \\ 0.022 & 0.023 & 0.057 \end{pmatrix}$$

$$\Theta_4 = \begin{pmatrix} 0.021 & -0.004 & -0.017 \\ 0.025 & 0.061 & 0.056 \\ -0.023 & 0.021 & 0.087 \end{pmatrix}$$

(d) $\mu = (105.89,\ 44.65,\ 89.50)$

$$\Sigma = \begin{pmatrix} 3.378 & 0.394 & 0.028 \\ 0.394 & 1.032 & 0.023 \\ 0.028 & 0.023 & 2.235 \end{pmatrix}$$

$$\Theta_1 = \begin{pmatrix} 0.410 & 0.039 & -0.019 \\ 0.086 & 0.271 & -0.020 \\ -0.036 & -0.006 & 0.062 \end{pmatrix}$$

$$\Theta_2 = \begin{pmatrix} 0.236 & -0.020 & 0.037 \\ -0.137 & 0.045 & 0.081 \\ 0.059 & 0.053 & 0.096 \end{pmatrix}$$

$$\Theta_3 = \begin{pmatrix} -0.172 & -0.021 & 0.019 \\ -0.013 & 0.029 & 0.018 \\ 0.037 & 0.028 & 0.044 \end{pmatrix}$$

$$\Theta_4 = \begin{pmatrix} 0.022 & -0.005 & -0.021 \\ 0.050 & 0.098 & 0.041 \\ -0.023 & 0.031 & 0.083 \end{pmatrix}$$

the northwestern directional pattern and, as it can be expected, it has a negative parameter in the northeast direction, which implies that its effect is suppressed. Each original sample and its corresponding synthesized realization are visually close and have similar characteristics as seen in Fig. 6. Also, the estimated values from the original realizations are numerically close to the specified values as shown in Table 2.

5. Conclusions

Even though texture is difficult to define, it is an important characteristic to perceive regions and surfaces. Texture analysis is successfully utilized in several applications such as segmentation and classification tasks in remote sensing and medical image analysis. For example, texture of forest, agricultural fields, lakes, and other land cover types in Landsat images can be identified in segmentation and classification tasks. Random field models, especially MRF models, have been usefully employed in texture modeling and sampling.

Since MRF is practically difficult to compute the probabilities of the joint distribution, relaxation-type algorithms are utilized instead of standard statistical procedures. Some subset of the parameter space causes phase transition in MRF that abrupt changes occur qualitatively and consequently leads to realizations dominated by one or two pixel values. Non-neighboring pixels lose the independency assumed in the MRF since local correlations grow during the relaxation type of algorithms. When phase transition occurs, as an alternative, iteration number is to be properly selected in sampling. which is based on visual interpretation, estimated parameters, the image size, and so on. For bigger images, a large number of iterations are required to obtain a stable texture.

Texture observed in mutichannel images such as remote sensing is usually related to the cross-channel correlation existing between bands as well as the spatial correlation within band, which should be taken into account in the model for it. The realizations shown in Section IV support that the variation in multispectral textured images is represented well using the GRMF model considering the spatial dependence between neighboring pixels.

Acknowledgements

The work described in this paper was supported by Anyang University Research Fund.

References

Chellappa, R., Kanal L. N., and Rosenfeld A., 1985. Two-dimensional discrete Gaussian Markov random field models for image processing, *Progress in Pattern Recognition*, 2: 79-112.

Cross, G. R. and A. K. Jain, 1983. Markov Random Field texture model, *IEEE Trans. Pattern Anal. Machine Intell.*, 5: 25-39.

Derin, H. and H. Elliot, 1987. Modeling of segmentation of noisy and textured image using Gibbs random field, *IEEE Trans. Pattern Anal. Machine Intell.*, 9:39-55.

Dubes, R. C. and A. K. Jain, 1989. Random field models in image analysis, *Journal of Applied statistics*, 16:131-164.

Geman, S. and D. Geman, 1984. Stochastic Relaxation, Gibbs Distribution, and the

Bayesian Restoration of Images, *IEEE Trans. Pattern Anal. Machine Intell.*, 6: 721-741.

Picard, Rosalind W., Elfadel, Ibrahim M., and Pentland, Alex P., 1991. Markov/Gibbs Texture Modeling;Aura Matrices and Temperature Effects, *IEEE Trans. Pattern Anal. Machine Intell.*, 5: 371-377.

Solberg, A. H., 1999. Contextual Data Fusion Applied to Forest Map Revision, *IEEE Trans. Geoscience and Remote Sensing*, 37(3):1234-1243.